Trans. Mat. Res. Soc. Japan 44[4] 143-148 (2019)

Three-dimensional X-ray topographic characterization of broken and unbroken natural diamond anvil crystals at 99.4 GPa

Kimihiko Morikawa[1], Kazuya Suzuki[1], Akane Fujimori[2], Shuntarou Takano[3], Satoshi Nakano[4], Hiroyuki Okamoto[5] and Kaoru Mizuno[1] *

1 Department of Physics and Materials Science, Shimane University, Matsue 690-8504, Japan
2 Department of Radiological Technology, Tsukuba International University, Tsuchiura 300-0051, Japan
3 Department of Physics, Kanazawa University, Kanazawa 920-1192, Japan
4 Ultra-High Pressure Group, National Institute for Materials Science, Tsukuba 305-0044, Japan
[5] School of Health Sciences, Kanazawa University, Kanazawa 920-0942, Japan
* Corresponding author: Fax: 81-852-32-6108, e-mail:mizuno@riko.shimane-u.ac.jp

Three-dimensional (3D) X-ray topography was used to characterize diamond anvil crystals before and after application of ultra-high pressure at 50, 70 and 99.4 GPa. The diffraction planes examined and the wavelength of the monochromatic X-rays were (004), (333), {224}, {440} and 0.0521 nm, respectively. Images of lattice defects in the diamond crystals were reconstructed by stacking approximately 500 X-ray limited projection topographs using the image processing software Image J. The 3D structures and nature of the lattice defects were identified from the reconstructed topographs. A pyramidal shape of four parts of stacking faults was identified using the visibility or invisibility of defect images with each diffraction plane. No significant changes of the lattice defects in the diamond crystals were observed under pressurization at 70 GPa. However, one of the anvil crystals shaped from the same rough crystal was broken into pieces at 99.4 GPa. The fracture stress is very low value rather than the calculated one based on (111) [110] slip system mechanism. In the broken crystal, the center line of plurality of the pyramidal shape of stacking faults differed in the location from the culet area. The breaking of diamond crystal was dependent on the distribution of plane defects in the crystal.

Key words: diamond, X-ray topography, anvil crystal, high pressure, lattice defect

1. INTRODUCTION

Diamond is the hardest known material and is used not only industrially for applications such as cutting tool blades, but also scientifically for various techniques.[1)] In particular, the invention of the diamond anvil cell (DAC) by Piermarini and Weir in 1962 and subsequent innovative improvement by Mao and colleagues in the 1970s made it possible to conduct extreme high pressure investigations.[2-7)] Many investigations using DACs in high-pressure physics have been reported.[8-10)] Furthermore, DACs have found many applications in geophysics and planetary sciences because they allow simulation of the pressure and temperature conditions of planetary interiors in the laboratory.[11-13)] During high-pressure experiments, one or both of the diamond anvil crystals are occasionally destroyed before reaching the target pressure. However, the reasons for such destruction of the diamond crystal have not yet been clarified. Theoretical studies on the strength of diamond crystal are of significant interest.[14-21)] A few experimental investigations using micro-indentation technique were reported and it is accepted that the plastic deformation in perfect synthesized crystal was {111}<110> slip mechanism.[22,23)] The real crystal strength is generally affected by lattice defects within the crystal. However, few investigations have been performed on lattice defects contained in natural diamond crystals, except those carried out using natural crystals by Lang.[24,25)] They observed only thin plate-like crystals and not bulk crystals due to the very low intensity of X-rays available. Some intrinsic defects, such as dislocations and stacking faults, were identified. In addition, diamonds were not suitable for investigations of plastic deformation due to their hardness. Synthesized diamond crystals with suitable size for X-ray topography were recently obtained by Sumitomo Electric Industries in Japan using a high-temperature, high-pressure synthesis method.[26,27)] Many investigations on the lattice defects in large synthetic diamond crystals have been carried out using X-ray topography with synchrotron radiation. In addition to the observation of stacking faults, the fault vectors of planar defects, Burgers vector and the nature of dislocation have been investigated.[28-40)]

However, natural diamond is used as an anvil crystal even now from the point of low price. In order to predict breaking pressure, it is necessary to investigate the relationship between the strength of the crystal and the nature and distribution of grown-in defects. There is no investigation that systematically tracked lattice defects in the diamond crystal until they were destroyed. Therefore, we observed changes of lattice defects in the natural diamond anvil crystals before and after application of ultra-high pressure by X-ray topography.

In X-ray topography, a three-dimensional (3D) defect structure is projected to two-dimensional detectors, such

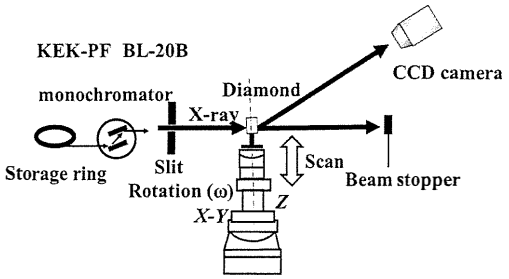

Fig. 1 Schematic diagram of the beamline (BL-20B, KEK-PF) and experimental setup for 3D topography with limited projection.

as a nuclear plate or CCD camera. Therefore, in principle, the location and orientation of defect remains arbitrary after re-construction of the defect structure and distribution. Many methods have been proposed to overcome this problem.[41-47] Andersen and Gerward reported the reconstruction of many limited projection topographs taken with step-scanning of a specimen crystal.[48] Recently, Kajiwara *et al.* applied 3D topography to the dislocation distribution of a necking area in a Czochralski grown silicon single crystal with a low dislocation density using white X-rays from a synchrotron radiation source.[49] Lattice defects are easier to observe by topography with a white X-ray beam than with monochromatic X-rays because the diffraction condition is much easier to hold by a continuous distribution of X-ray wavelengths. However, the resolution power of white X-ray topographs is lower than that of monochromatic X-ray topographs. Therefore, we have used a monochromatic X-ray beam instead of a white X-ray beam for topography, although there are technical difficulties, such as precise holding of the diffraction condition for a long time. 3D X-ray topography with top-up operation of the storage ring was used to characterize a natural diamond anvil crystal before and after pressurization in an anvil cell for high-pressure experiments.

2. EXPERIMENTAL PROCEDURES

Topographic observation by limited projection was conducted at the white X-ray beam station (BL-20B) of the Photon Factory (PF) located at the High Energy Accelerator Research Organization (KEK) in Tsukuba, Japan. A Si(111) double-crystal monochromator in the beam line was used to produce 0.0521 nm X-rays from white X-rays generated from the bending magnet in the storage ring under top-up operation where a continuous

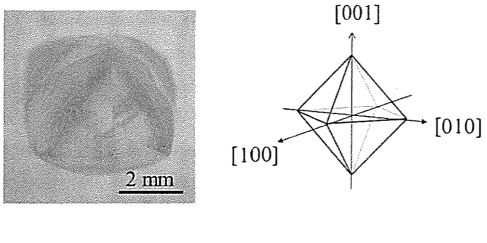

Fig. 2 (a) Photograph of rough diamond crystal and (b) its orientations.

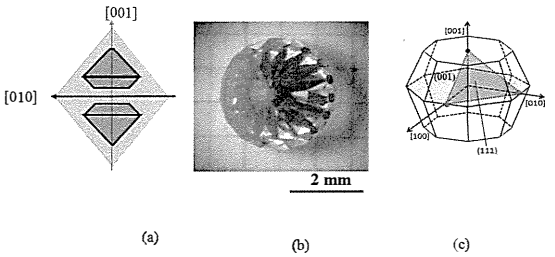

Fig. 3 (a) Cutting position of diamond anvil crystals from a rough crystal, (b) photograph of the shaped anvil crystal and (c) its orientations.

injection of electrons is employed to maintain a constant accumulated current.[50] The experimental setup for the present investigation is shown in Fig. 1. The principle of 3D topography using a number of limited projection topographs was proposed by Andersen and Gerward.[48] In this technique, several hundred topographs must be acquired under the exact same diffraction condition. It is very difficult to obtain topographs with monochromatic X-rays unless the top-up operation is employed. The acceleration voltage and constant beam current of the storage ring were exactly 2.5 GeV and 400 mA, respectively. The cross-sectional size of the X-ray beam used for sectional topographs was 10 μm × 10 mm. The diffraction planes of the specimen were four equivalents: {224}, {440}, {333} and (004). The diffraction images were recorded with a CCD camera (Photonic Science Inc., XFDI). The pixel size was 6.7 μm × 6.7 μm, and the size of each image was 1383 pixels × 1032 pixels. The exposure time was approximately 7 s. The specimen was elevated by 10 μm after acquisition of each topograph, and this was repeated for each observation. The number of topographs for each observation was approximately 500. Lattice defect images of diamond crystals were reconstructed from stacking of approximately 500 sectional X-ray topographs using the image processing software Image J. An arbitrary crystal plane cut from the reconstructed image was observed. Details of this technique have been already published elsewhere.[40]

Natural octahedral rough diamond crystals used in the present investigation were supplied by Syntek Co., Ltd., Japan. Diamond crystal used as a specimen was type Ia. Figure 2 shows a photograph of a rough diamond crystal and the orientation. After X-ray topographic observation, the rough crystal was cut in two symmetrical Drucker-Prager type anvil crystals and polished. The size of the specimen was 3.5 mm in girdle diameter, 2 mm in height and 0.3 mm in culet diameter. Figure 3 shows a photograph and orientations of the shaped crystal specimen. The crystal axis of both anvil diamond crystals in the pressure direction was [001]. After topographic observation of the two diamond anvil crystals, the diamond crystals were attached to an anvil cell. Argon gas as a pressure medium and ruby chips as a pressure marker were introduced into a sample chamber, which consists of a 70 μm thick rhenium gasket with a 150 μm diameter hole and a pair of diamond anvils. Pressure value was determined by ruby fluorescence method. The pressure was elevated to 50 GPa and then released, and the diamond crystals were removed from the anvil

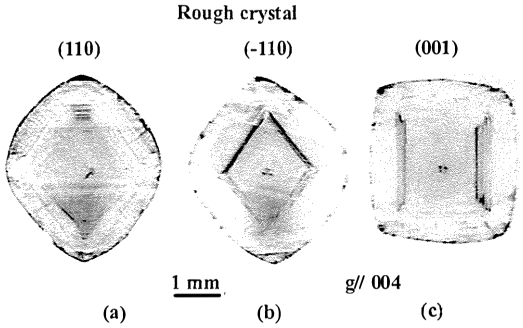

Fig. 4 (a) (110), (b) (1-10) and (c) (001) cross-sectional views of the 3D reconstructed topographs of the rough diamond crystal for the (004) diffraction plane.

cell for further 3D topograph observations. No change in the appearance of the anvil crystals due to pressurization of 50 GPa was observed; therefore, the crystals were attached to the anvil cell again and pressurized to 70 GPa. After the pressure was released and 3D topographs were acquired, the diamond crystals were then pressurized to 99.4 GPa. At 99.4 GPa, one of the anvil crystals was broken into pieces.

3. RESULTS AND DISCUSSION

All limited projection topographs were shrunken along the direction of the incident X-ray beam, due to the asymmetric reflection of the specimen. After this correction, all limited projection topographs were stacked to construct a 3D image using Image J. The 3D image was then finally converted into a cross-sectional view along an arbitrary crystal plane.[40] Figure 4 shows (110), (1-10) and (001) cross-sectional views of the rough diamond crystal taken from the reconstructed 3D topograph using the diffraction plane (004). Lozenge images shown in Figs. 4(a) and (b) and the rectangular image in (c) indicate an octahedral planar defect on the {111} plane as shown latter in the rough diamond crystal. Identification of the nature of plane defects was conducted after shaping the crystal to the anvil.

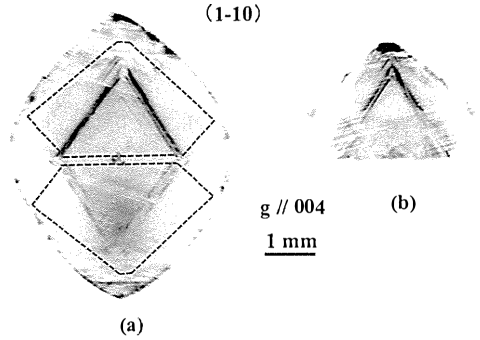

Fig. 5 (a) (1-11) cross-sectional views of the rough diamond and (b) the diamond anvil crystal for the (004) diffraction plane. The diamond anvil crystal was cut according to the dotted lines shown on the rough crystal in (a). Strain at the top area of the anvil crystal appeared due to shaping of the crystal.

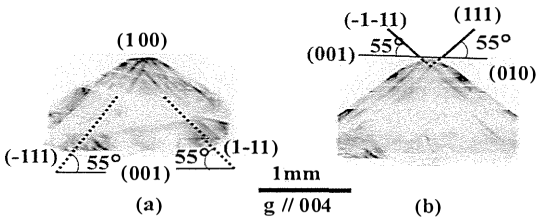

Fig. 6. (a) (100) and (b) (0-10) cross-sectional views of the anvil crystal. The topographs show two symmetrically inclined lines formed by at 55° with a horizontal line on (001). The straight lines formed at 55° with (100) are located on the {111} plane.

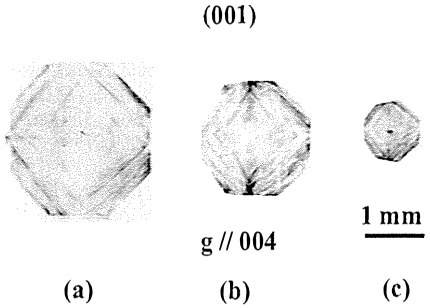

Fig. 7. (001) cross-sectional view of the 3D reconstructed topograph at different heights of the crystal. Defects observed as lines in Fig. 6 are considered to be planar defects on {111}.

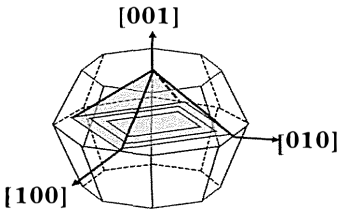

Fig. 8. Schematic diagram of quadrangular pyramids formed by planar defects on (111).

Two symmetric Drucker-Prager type anvil crystals were cut from the rough crystal, as shown by dotted line in Fig. 5(a), and then polished. Figure 5(b) shows a (1-10) cross-sectional view of the diamond anvil crystal with the (004) diffraction plane. Almost all defects evident in Fig. 5(b) were observed to be the same as inFig. 5(a). However, strong strain contrast was observed at the top of the anvil (culet). Before shaping the anvil crystal, no strain was evident near the culet, as shown in Fig. 4. Therefore, the strain near the culet was introduced by the cutting and polishing procedures. However, plastic deformation during shaping of the anvil crystal was not observed in other areas. Unfortunately, details of the procedures conducted by Syntek Co. were undisclosed; therefore, the cause of the induced strain near the culet could not be clarified.

Next, the nature of the defects observed as lines in the anvil crystals was identified. Figures 6(a) and (b) show (110) and (1-10) cross-sectional views of the specimen crystal with the (004) diffraction, respectively. The topographs show two symmetrical inclined lines formed at 55° with a horizontal line on (001). From geometrical consideration, the straight lines formed at

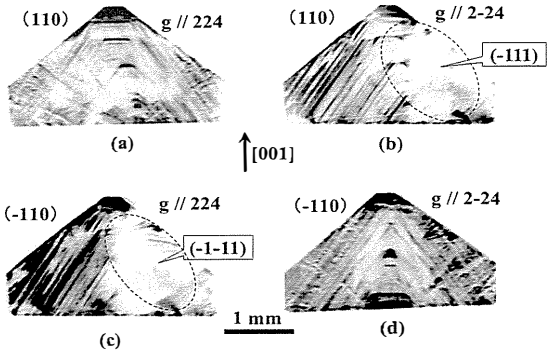

Fig. 9 (a,b) (110) and (c,d) (-110) cross-sectional views of the anvil crystal reconstructed from (a,c) (224) and (b,d) (2-24) diffraction topographs, respectively. The inclined line images framed by the dotted ellipsoid were invisible in (b) and (c). Defect images show the dependence of visibility or invisibility on the diffraction plane.

55° with (001) are located on the {111} plane. Furthermore, these lines were observed for other cross-sectional views on the {110} plane, as shown in Fig. 6(b). Therefore, defects observed as lines in Fig. 6 are considered to be planar defects on the {111} plane. Figure 7 shows the (001) cross-sectional view of the 3D reconstructed topograph at different heights of the crystal. The cross-sectional view from (001) of planar defects on the (111) plane could be observed as rectangular lines parallel to <110>, as shown in Figs. 7(a), (b) and (c). Therefore, the defect shape observed in the topographs was estimated to be a pyramidal form as shown schematically in Fig. 8.

The present results suggest that the quadrangular pyramids are formed by planar defects on (111), as shown in Fig. 8. The defect was then examined with respect to four equivalent {440} and {224} diffraction planes. The nature of the defect was determined by determining the reflection in which the planar defects become invisible. To identify the nature of the planar defects, visibility of the defects in {111} was first determined with the different but equivalent diffraction {224} plane. Figures 9(a) and (b) show (110) cross-sectional views of the reconstructed 3D topograph for the (224) and (2-24) diffraction planes, respectively. Figures 9(c) and (d) show (-110) cross-sectional views for the (224) and (2-24) diffraction planes, respectively. The upward and downward sloping lines in Fig. 9 show the cross-section of planar defects on {111}.

Figures 10(a), (b), (c) and (d) show (001) cross-sectional views of the reconstructed 3D topographs for the (404), (-404), (044) and (0-44) diffraction planes, respectively. There are many lines with four <111> directions originated with a plurality of pyramidal shape plane defects in the (001) cross-section; however, only two lines are evident with the diffraction conditions, as shown in Fig. 10. Table I provides a summary of the visible (○) or invisible (×) planar defects for the different diffraction planes and the results agree with the calculated inner product with diffraction vector, **g** and normal vector of fault plane, **u**. If no defect was observed, then the diffraction vector and the normal vector of planar defects were perpendicular to each

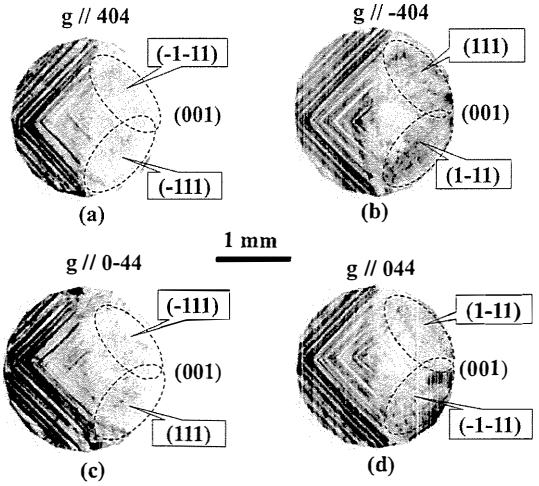

Fig. 10 (001) cross-sectional views of the anvil crystal reconstructed from (a) (404), (b) (-404), (c) (0-44) and (d) (044) diffraction topographs. The two inclined line images framed by the dotted ellipsoids were invisible in all topographs. Defect images showed the dependence of visibility or invisibility on the diffraction plane.

Table I. Summary of visible and invisible images of the plane defect: (○) visible and (×) invisible.

g·u		Diffraction vector g							
		[224]	[2-24]	[-2-24]	[-224]	[404]	[0-44]	[-404]	[044]
u	[111]	○	○	×	○	○	×	×	○
	[1-11]	○	○	○	×	○	○	×	×
	[-1-11]	×	○	○	○	×	○	○	×
	[-1-11]	○	×	○	○	×	×	○	○

other.[51] Planar defects were not observed on only two of the equivalent four (111) planes, as shown in Fig. 10. The results given in Table I indicate that the planar defect on (111) is a stacking fault, as shown previously.[32] However, it was impossible to determine the type of stacking fault, Frank or Shockley type, by the present experiment. The fringe pattern often encountered in a stacking fault is not observed in Figs. 4 and 5. It is thought that the fringe pattern cannot be observed owing to the low resolution power of the present method.

Figure 11 shows (110) cross-sectional views of the 3D reconstructed topographs of the specimen crystal for the (3-33) diffraction (a) before high-pressure application, and after high-pressure application at (b) 50 GPa, (c) 70 GPa and (d) 94.4 GPa. This diamond crystal was not broken at 99.4 GPa. No significant change of the stacking faults due to the applied high pressure could be observed in the topographs although local strong strain image around the stacking faults was observed. The number density of stacking fault obtained from Fig.11 (a) was 5 mm^2/mm^3.

Figure 12 shows topographs similar to those in Fig. 11, except that the specimen crystal was broken into pieces at 99.4 GPa. However, the lattice defects shown in Fig. 12 did not change, as was the case in Fig. 11; therefore, plastic deformation of the diamond crystal did not occur under application of pressure at 70 GPa. The number density of stacking fault obtained from Fig.12 (a) was 7 mm^2/mm^3. There was no significant difference in stacking fault density between the broken crystal and the unbroken crystal.

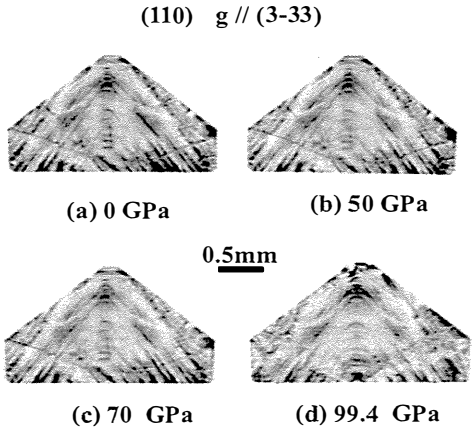

Fig. 11 (110) cross-sectional views of the 3D reconstructed topograph of the specimen crystal with (3-33) diffraction before (a) application of high pressure, and after application of high pressure at (b) 50 GPa, (c) 70 GPa and (d) 99.4GPa. This diamond crystal was not broken at 99.4 GPa.

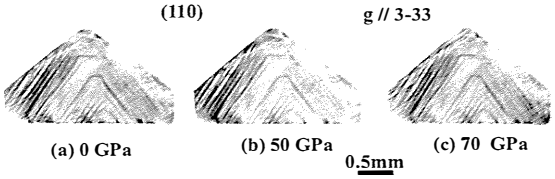

Fig. 12 (110) cross-sectional view of the 3D reconstructed topograph of the specimen crystal with (3-33) diffraction before (a) application of high pressure, and after application of high pressure at (b) 50 GPa and (c) 70 GPa. The diamond crystal was broken into pieces at 99.4 GPa.

Figure 13 shows the topographs for the unbroken diamond crystal and the crystal broken at 99.4 GPa. For the unbroken crystal, the center line of the plurality of pyramidal-shape stacking faults (dashed line) overlapped with each other is shown within the culet, as in Fig. 13(a). However, for the broken crystal, the center line of the pyramidal-shape stacking faults differs in location and moves from the culet as shown by the dashed lines in Fig. 13(b). These diamond crystals were shaped from the same rough diamond crystal and they had the almost same stacking fault density. However, minor differences in the distribution of the stacking faults after shaping were observed. As the deviation in location of the pyramidal-shape stacking faults is observed only broken crystal, it is introduced to the crystal by the fluctuation of growth condition during the growth process. The breaking strength of the diamond anvil crystal was thus dependent on the distribution of lattice defects.

Next, we discuss the critical shear stress acting on (111) face in order to clarify the influence of grow-in lattice defects to the crystal strength. It is well known that the critical shear stress τ, resolved on the slip plane in the slip direction, is

$$\tau = \frac{F}{A}\cos\varphi \sin\lambda, \qquad (1)$$

where F is the applied compressive force, A is the

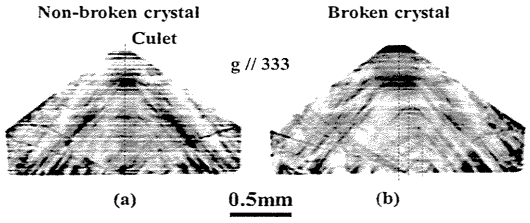

Fig. 13 Difference between the topographs for (a) the unbroken diamond crystal and (b) the crystal broken at 99.4 GPa.

cross-sectional area, φ is the angle between F and the normal of slip plane and λ is the angle between F and the slip direction.[51] In the present study, direction of the compressive force is [001] and the slip direction is <110> on {111}, so φ=54.7° and λ=45.0° . Since the applied stress is 99.4 GPa, maximum value of critical share stress is $\tau = 41 \times 10^9$ N/m^2. Tyson reported that the calculated critical shear stress for diamond crystal on (111) is 125×10^9 N/mm^2 using Peierls mechanism.[52] The critical shear stress obtained present experiment is less than a half of the Tyson's value. Therefore, present destruction of the crystal was subjected to lattice defects other than dislocation lines, may be staking fault.

4. CONCLUSIONS

Natural diamond anvil crystals shaped from the same rough crystal were characterized using 3D X-ray topography with a monochromatic beam. Planar defects on {111} were observed and were identified as stacking faults. No significant change of the lattice defects in the diamond crystals was observed under pressurization at 70 GPa. However, one of the anvil crystals was broken into pieces at 99.4 GPa. In the broken crystal, the center line of the plurality of pyramidal-shape stacking faults differed in location from the center of the culet area. The breaking strength was thus confirmed to be dependent on the distribution of lattice defects in the diamond crystal. In order to obtain an anvil crystal that can withstand high pressure, it is necessary to evaluate lattice defects inside the crystal and to select an ore having a highly symmetrical defect distribution.

Acknowledgement

This study was conducted with the approval of the Photon Factory Advisory Committee (Proposal Nos. 2013G608 and 2015G561).

References:

[1] A. Kelly and N. H. Macmillan, *Strong Solids* (Clarendon, Oxford, 1986).
[2] G. J. Piermarini and C. E. Weir, J. Res. Natl. Bur. Stand. Sect. A**66**, 325(1962).
[3] H. K. Mao and P. M. Bell, Science, **191**, 851(1976).
[4] H. K. Mao and P. M. Bell, Science, **200**, 1145(1978).
[5] K. A. Goettel, H. K. Mao, and P. M. Bell, Rev. Sci. Instrum., 56, (1985)1420.
[6] H. K. Mao, Y. Wu, L. C. Chen, J. F. Shu, and A. P. Jephcoat, J. Geophys. Res. **95**, 21737(1990).
[7] A. Jayaraman, Rev. Sci. Instrum.,57, 1013(1986).
[8] S. Nakano, R. J. Hemley, E. A. Gregoryanz, A. F. Goncharov, and H. K. Mao, J. Phys., Condensed Matter.

14,10453(2002).
[9] T. Moriwaki, Y. Akahama, H. Kawamura, S. Nakano, and K. Takemura, J. Phys. Soc. Jpn. **75,** 074603 (2006).
[10] S. Nakano, H. Fujihisa, H. Yamawaki, and T. Kikegawa, J. Phys. Chem. C. **119,** 3911 (2015).
[11] H. K. Mao and W. L. Mao, Treatise on Geophysics, 2nd ed., (Elsevier, Amsterdam, 2007), p.231.
[12] A. Sano-Furukawa, H. Kagi, T. Nagai, S. Nakano, S. Fukura, D. Ushijima, R. Iizuka, E. Ohtani, and T. Yagi, American Mineralogist. **94,** 1255 (2009).
[13] A. Shinozaki, H. Kagi, H. Hirai, H. Ohfuji, T. Okada, S. Nakano, and T. Yagi, Phys. Chem. Mineals. **43,** 277 (2016).
[14] D. Nelson, Jr. and A. L. Ruoff, J. Appl. Phys., **50**, 2763(1979).
[15] A. L. Ruoff, J. Appl. Phys., **50**, 3353(1979).
[16] M. S. Bruno and K. J. Dunn, Rev. Sci. Instrum., **55**, 940(1984).
[17] W. C. Moss, J. O. Hallquist, R. Reichlin, K. A. Goettel, and S. Msrtin, Appl. Phys. Lett., **48**, 1258(1986).
[18] S. Merkel, R. J. Hemley, and H. K. Mao, Appl. Phys. Lett., **74**, 656(1999).
[19] J. J. Zhao, S. Scandolo, J. Kohanoff, G. L. Chiarotti, and E. Tosatti, Appl. Phys. Lett., **75**, 487(1999).
[20] R. H. Telling, C. J. Picard, M. C. Payne, and J. E. Field, Phys. Rev. Lett., **84**, 5160(2000).
[21] H. Chacham and L. Kleinman, Phys. Rev. Lett., **85**, 4904(2000).
[22] C. A. Brookes, Nature **228**, 660 (1970).
[23] H. Sumiya, K. Yamaguchi and S. Ogata, Appl. Phys. Lett., **88**, 161904 (2006).
[24] A. R. Lang, J. Cryst. Growth **24-25**, 108(1974).
[25] B. K. Tanner, *X-ray Topography*, (Pergamon Press, Oxford, 1976) p. 145.
[26] H. Sumiya and S. Satoh, Diamond Relat. Mater. **5**, 1359 (1996).
[27] H. Sumiya, J. Cryst. Growth **178**, 485 (1997).
[28] W. Wierchowski and M. Moor, Acta Phys. Pol. A **82**, 185 (1992).
[29] A. R. Lang, Diamond Relat. Mater. **2**, 106 (1993).
[30] A. Yacoor and M. Moor, Mine.Mag. **57**, 223 (1993).
[31] A. R. Lang, J. Appl. Crystallogr. **27**, 988 (1994).
W. Wierchowski and M. Moor, Acta Crystallogr. Sect. A: **51**, 831 (1995).
[32] G. Kowalski, M. Moore, G. Gledhill, and Z. Maricic, Diamond Relat. Mater. **5**, 1254 (1996).
[33] M. Moor and W. Wierchowski, Philos. Trans. R. Soc. London. A**357**, 2671 (1999).
[34] M.Moor, J. Phys.: Condens Matter **21**, 364217 (2009).
[35] H. Sumiya and K. Tamasaku, Jpn.J.Appl.Phys.**51,** 090102 (2012).
[36] Y. Kato, H. Umezawa, H. Yamaguchi, and S. Shikata, Jpn. J. Appl. Phys.**51**, 090103 (2012).
[37] M. Kasu, R. Murakami, S. Masuya, K. Harada, and
[38] H. Sumiya, Appl. Phys. Express **7**,125501 (2014).
[39] M. Moor, S. G. Nailer, and W.Wierchowski, Crystals **6**, 71 (2016) .
[40] K. Mizuno, K. Suzuki, H. Un-no, K. Morikawa and H. Okamoto, Jpn. J. Appli. Phys. **57**, 085503(2018).
[41] A. R. Lang, Acta. Crystallogr. **12**, 249 (1959).
[42] A. R. Lang, J. Appl. Phys. **30**, 1748 (1959).
[43] K. Haruta, J.Appl.Phys. **36**,1789 (1965).
[44] B. K. Tanner and D. K. Bowen, *Characterization of Crystal Growth Defects by X-ray Methods* (Plenum Press, New York, 1980) p. 170.
[45] W. Ludwig, P.Cioetens, J. Härtwig, J. Baruchel, B. Hamelin, and P. Bastie, J. Appl. Crystallogr. **34**, 602 (2001).
[46] S. Kawado, T. Taishi, S. Iida, Y. Suzuki, Y. Chikaura, and K. Kajiwara, J. Synchrotron Radiat. **11**,304 (2004).
[47] S. Kawado, T. Taishi, S. Iida, Y. Suzuki, Y. Chikaura, and K. Kajiwara, J. Phys. D **38**,A17 (2005).
[48] A. L. Andersen and L. Gerward, Phys. Status Solidi A **23**, 537 (1974).
[49] K. Kajiwara, S. Kawado, S. Iida, Y. Suzuki, and Y. Chikaura, Phys. Status Solidi A **204**, 2682 (2007).
[50] S. Nakamura, M. Ohno, N. Awaji, A. Chiha, R. Kitano, H. Nishizawa, O. Asai, M. Takanaka, T. Iida, Y. Yamamoto, M. Shiota, M. Mizota, S. Kawazu, M. Kodaira, K. Kondo, and T. Tomimasu, Proc. 2nd European Particle Accelerator Conf., 1990, p. 472.
[51] D. Hall and D. J. Bacon, *Introduction to dislocations 3rd ed.*, (Pergamon Press, Oxford, 1984).
[52] W. R. Tyson, Philos. Mag., **131**, 925 (1966).

(Received February 9, 2019; Accepted June 29, 2019;
Published Online August 1, 2019)